TD-05-008
2/16/05

Fermi National Accelerator Laboratory
Technical Division
PO Box 500 MS 316
Batavia, IL 60510

Modeling and Parametric Studies of the MTF Cold Box

R. Rabehl

Abstract:

An equation-based model of the MTF cold box has been developed to aid in maximizing performance (i.e., liquefaction rate) of the MTF liquid helium plant. Development of the model is discussed, and predicted performance results are presented. Of the parameters investigated, compressor discharge pressure and storage dewar pressure offer the greatest opportunities for system performance improvement.

1. Introduction

Commissioned in the late 1970's, the MTF liquid helium plant has provided reliable operation beginning with Tevatron superconducting magnet production testing and up to and including today's LHC quadrupole production testing and high-field magnet R&D testing. Recent years have seen a high demand on the cryogenics system and a need to improve its performance, specifically by simultaneously supporting multiple cold test stands.

A model of the MTF cold box has developed based on characteristics documented in TD-05-007, "Operational Characteristics of the MTF Liquid Helium Plant." Descriptions of component models and their integration into a system model are discussed.

Using this model, a series of parametric studies were conducted to investigate the effect of various system parameters on liquefaction rate. These results are presented with a discussion of the impact of these parameters on cryogenic operations.

2. MTF Cold Box Model

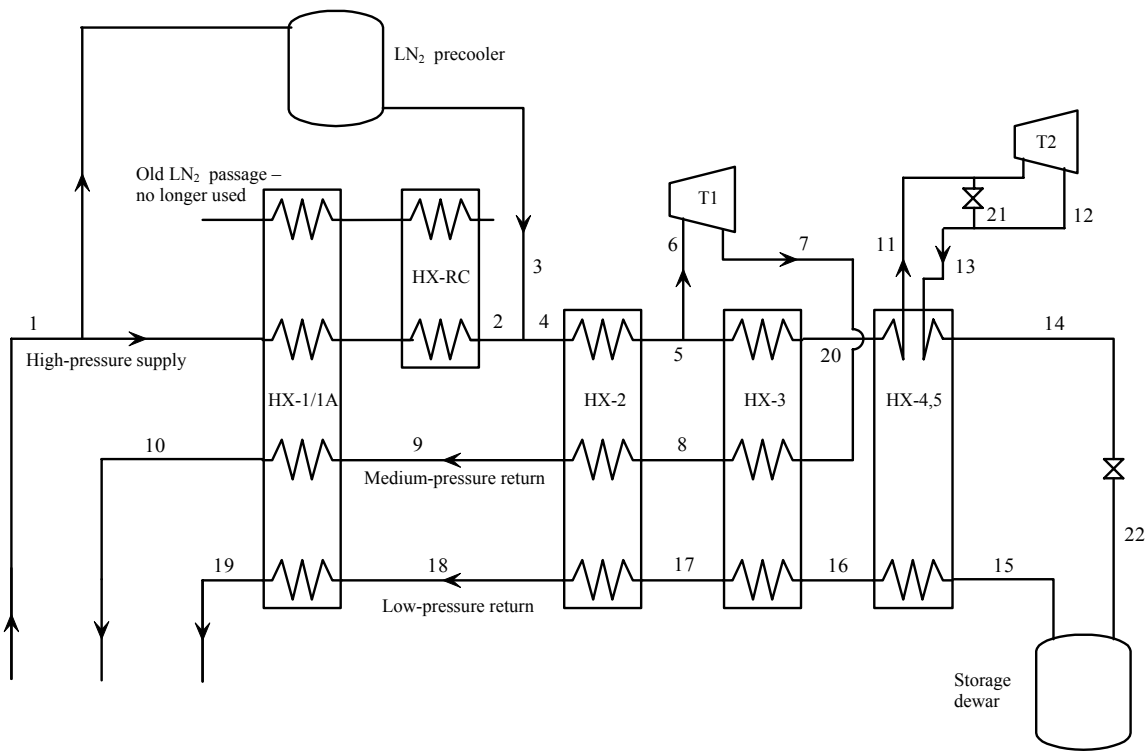

Figure 1 Schematic and numbered state points of the MTF cold box model.

Figure 1 shows the schematic and numbered state points of the MTF cold box model. There are a total of 22 state points where pressure, temperature, and other thermodynamics properties are calculated as required. The model includes four heat

exchanger packages (since the old LN_2 passages are no longer used in heat exchangers HX-1/1A and HX-RC, HX-RC is no longer active), the external LN_2 precooler, expansion turbines T1 and T2, two valves, and the 10,000 l storage dewar. Conditions at each state point are calculated with mass and energy balances and, in some cases, isentropic efficiency calculations. The model is equation-based and written in the Engineering Equation Software (EES) [1] program. Helium properties are determined using an external procedure called HeProp, which uses data from the popular Hepak program [2]. The model contains over 200 equations.

There are a number of inputs for the model: LN_2 precooler GHe flow rate, pressures of the high-, medium-, and low-pressure streams, turbine efficiencies, storage dewar pressure, high-pressure supply temperature, the precooler GHe outlet temperature, flow rate through the T2 bypass valve PCV56, and cold return flow from the distribution box and magnet test stands. The LN_2 precooler GHe flow rate simulates control loop TIC1530, which regulates the precooler helium flow rate to maintain a given temperature at state point 2. This setpoint is normally about 108 K. Cold return flow allows investigation of system performance when it is operated as a refrigerator, a liquefier, or somewhere in between.

Static heat loads of the cold box, storage dewar, and transfer lines are not included in the model.

2.1 Model Component – High-Pressure Flow to Cold Box

An important parameter required by the model is the mass flow rate to the cold box. As discussed elsewhere [3], the flow rate is determined by the turbine inlet valves, the turbines themselves, and the T2 bypass valve PCV56. The equations of the system model do not converge when the mass flow rate to the cold box is calculated based on the turbine inlet conditions, however.

Instead, logged operating data was collected to look for a relationship between compressor discharge pressure and the mass flow rate to the cold box. Figure 2 shows this relationship for logged operating data from the periods of January-February 2004 and August-September 2004. The cold box mass flow rate is calculated based on measured conditions at a compressor skid orifice plate. At compressor discharge pressures of 200 psia and higher, there is not much spread in the data. The spread becomes greater at lower compressor discharge pressures as more adjustments are made to ‘balance out the machine’ (reduce the liquefaction rate to match the system load): turbine inlet valves are partially closed, turbines are slowed down, and the T2 bypass valve may be opened. There is also some spread simply due to the mass flow calculation at the orifice plate. It is expected that points near the upper portion of the scatter would correspond to operation with the turbine valves fully open to maximize liquefaction. However, applying such a relationship to the model again leads to convergence problems. A relationship shown by the red line was used instead.

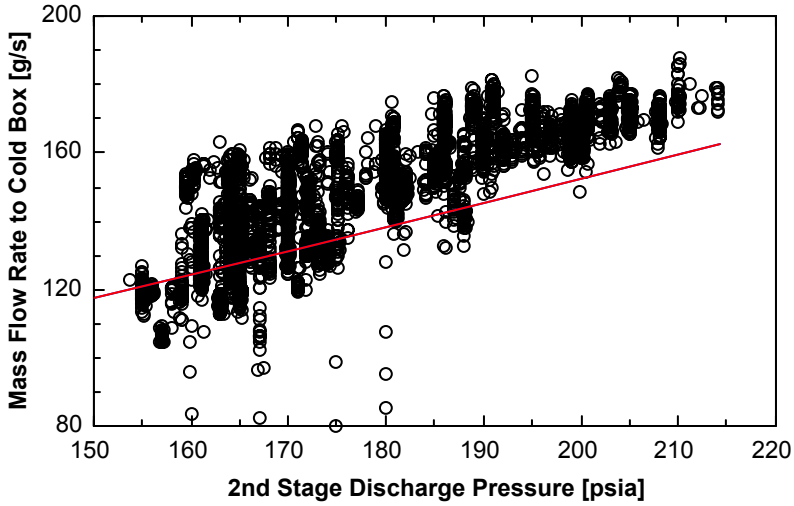

Figure 2 Logged operating data showing the relationship between second stage discharge pressure and mass flow rate to the cold box. The red line indicates the relationship used in the cold box model.

2.2 Model Component – Heat Exchangers

The cold box contains seven heat exchangers in four packages: HX-1 and 1A in one package, HX-RC in a second package (inactive), HX-2 in a third package, and HX-3, 4, and 5 in the fourth package. In this model, HX-1/1A, HX-2, HX-3, HX-4, and HX-5 are treated as individual heat exchangers as shown in the schematic of Figure 1.

Heat exchangers generally can be analyzed using either the UA-LMTD method or the ε-NTU method. The UA-LMTD method is usually used in designing a heat exchanger with known inlet conditions and desired outlet conditions. In contrast, the ε-NTU method is used to analyze a given heat exchanger with known inlet conditions. The ε-NTU method is used in this model with an assumed effectiveness ε =1 for all heat exchangers. Heat exchange between two fluid streams is then determined using Equations 1 and 2:

$$C_{min} = \min\left[\left(\dot{m}\, c_p\right)_h, \left(\dot{m}\, c_p\right)_c\right] \tag{1}$$

$$q = \varepsilon\, C_{min}\left(T_{h,i} - T_{c,i}\right) \tag{2}$$

where $\dot{m}$ is the mass flow rate, c_p is the specific heat, C_{min} in the minimum thermal capacitance, T is the temperature, ε is the heat exchanger effectiveness, q is the heat transfer rate, and the subscripts h and c denote the hot and cold streams, respectively.

HX-4 and HX-5 provide heat transfer surface between the high-pressure supply stream and the low-pressure return stream. Only two fluids are involved, and the analysis is

straightforward. HX-1/1A, HX-2, and HX-3 all provide heat transfer surface between the high-pressure supply stream, the medium-pressure return stream, and the low-pressure return stream. The analysis is not so straightforward when three fluids are involved; most existing models are complex and require detailed knowledge of the heat exchanger construction and geometry [4-5]. Not yet included in this system model, the author will attempt to construct a more general heat exchanger model using another method [6] where geometric terms are lumped together into characteristic parameters, which are then fit to operating data.

To simplify the heat exchanger model within the larger cold box model, each three-fluid heat exchanger is broken into two two-fluid heat exchangers as shown in Figure 3. The high-pressure supply stream is equally divided; one half exchanges heat with the medium-pressure return stream, and the other half exchanges heat with the low-pressure return stream. The two high-pressure streams then recombine and mix to yield the final state at the three-stream heat exchanger outlet.

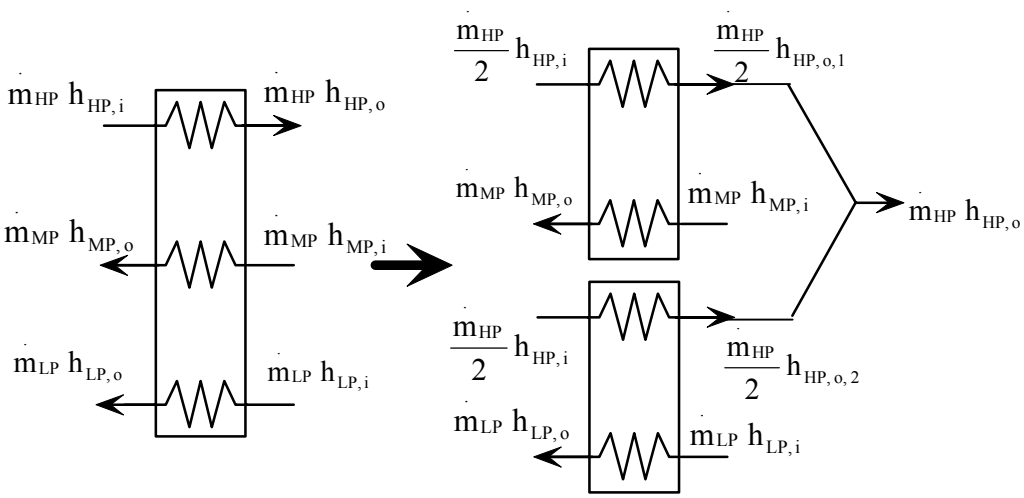

Figure 3 Three-stream heat exchanger model.

2.3 Model Component – Turbine Flow and Performance

As described elsewhere [3], empirical relationships for the flows through the T1 and T2 turbines have been determined. The T1 flow equation was determined using flow rates calculated from a downstream venturi. The T2 flow equation was determined using a mass balance with the flow rate entering the cold box and the T1 flow rate. These relationships are repeated as Equations 3 and 4:

$$\text{T1 flow:}\quad \dot{m}\,[\text{g/s}] = 1.32\sqrt{\rho_{in}\,[\text{kg/m}^3]\,P_{in}\,[\text{psia}]} \tag{3}$$

$$\text{T2 flow:}\quad \dot{m}\,[\text{g/s}] = 0.753\sqrt{\rho_{in}\,[\text{kg/m}^3]\,P_{in}\,[\text{psia}]} \tag{4}$$

where $\dot{m}$ is the mass flow rate, ρ_{in} is the turbine inlet density, and P_{in} is the turbine inlet pressure.

As discussed earlier, these relationships were not able to be directly applied in the model due to convergence problems. Instead, the flow rate entering the cold box as indicated by Figure 2 and the T1 flow rate as indicated by Equation 3 are used. The difference then goes through T2 and its bypass valve PCV56. The flow rate entering the cold box is lower than indicated by operating data, and the result is a T2 flow rate that is lower than that expected by Equation 4. Convergence problems were again encountered when reducing the T1 flow rate so that the correct ratio of T1 flow rate to flow rate entering the cold box was maintained.

Turbine performance measures (i.e., isentropic efficiencies) are inputs to the model. Typical T1 turbine performance data are presented elsewhere [3]. T2 turbine performance data are not available because the inlet and outlet temperatures are not measured accurately enough for meaningful efficiency calculations. Calculated isentropic efficiencies for the T2 turbine tend to be either greater than one or less than zero. Assumed T2 turbine efficiencies are based on the slower speed of T2 relative to T1 and its smaller expander wheel.

3. Cold Box Model Parametric Studies

A number of parametric studies were run with the model to study the influence of various system parameters. The results of these studies can point toward system improvements/modifications and operational changes to increase flexibility of the cryogenics system. The implications of each parameter on system operations are discussed as well.

The baseline conditions for the model are listed in Table 1.

Table 1 Baseline conditions for the cold box model.

Parameter	Value
2nd stage compressor discharge pressure	200 psia
Storage dewar pressure	23.4 psia
T1 turbine isentropic efficiency	0.7
T2 turbine isentropic efficiency	0.5
T2 turbine bypass flow through PCV56	0 g/s
Cold return flow	0 g/s

3.1 Compressor Discharge Pressure

Figure 4 shows the predicted effect of compressor discharge pressure on relative liquefaction rate when operating in liquefier mode. There is a strong dependence;

operating at higher compressor discharge pressures significantly increases the liquefaction rate. This is due to two effects. First, more mass is pushed through the cold box as compressor discharge pressure increases. Second, the pressure ratio across each turbine is increased so more expansion work is removed from the high-pressure process stream.

Operating at higher compressor discharge pressures has a number of implications. Increasing the mass flow to the cold box means that the mass flow returning to the compressors will also increase. The slide valve change-out during the March 2005 maintenance shutdown is expected to allow 20% higher throughput through the first stage compressor with reduced motor current, allowing low suction pressures to be maintained. The gas management system can also be a limiting factor in compressor discharge pressure. Some gas is recirculated from the second stage discharge in order to maintain interstage pressure. Installing a new buffer-to-interstage gas management valve with a higher C_v value would minimize this recirculation of gas. The higher first stage compressor throughput after the slide valve change-out also will reduce gas recirculation around the second stage compressor. Operation of the compressor cooling system is another important factor in running at higher compressor discharge pressures. Limits of the glycol system have not been fully explored. Finally, there are electrical considerations when running at higher compressor discharge pressures. The 1000 hp motor has a full-load current of nearly 1100 A, but its breaker is set at 960 A due to power factor issues.

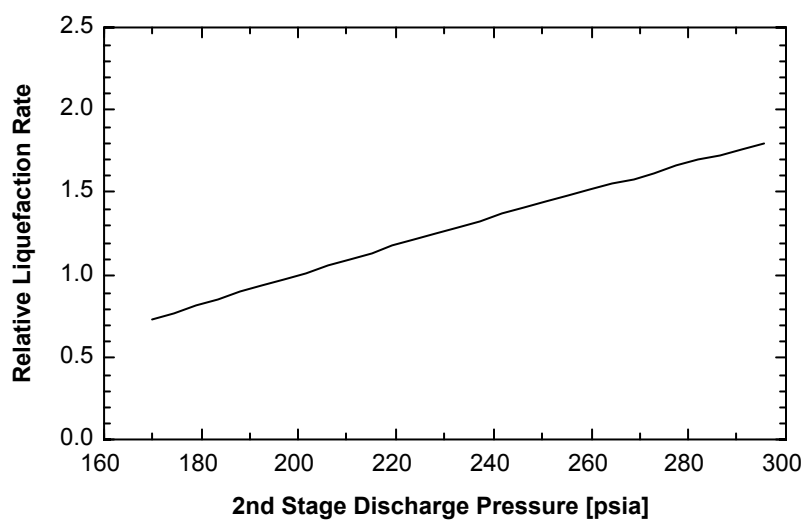

Figure 4 Predicted relative liquefaction rate as a function of second stage compressor discharge pressure.

3.2 Storage Dewar Pressure

Figure 5 shows the predicted effect of storage dewar pressure on relative liquefaction rate when operating in liquefier mode. A 1 psi reduction in storage dewar pressure increases the liquefaction rate by approximately 10%.

The slide valve change-out during the March 2005 maintenance shutdown is expected to allow better control over storage dewar pressure. Current compressor operations result in suction pressure ranging anywhere from 17.5 psia to 22 psia depending on which test stand is being supported and at what temperature. The storage dewar pressure then varies as well. Control loop PIC300 controls storage dewar pressure by venting helium gas to compressor suction and is typically run in manual mode. The control loop is slow due to the large volume of the storage dewar, and running it manually minimizes pressure swings as suction pressure varies. However, running PIC300 manually also allows the storage dewar pressure to creep during longer periods of steady plant operations. The expected increase in first stage compressor throughput will allow suction pressure to remain more stable and should allow PIC300 to be run in automatic mode more often. This will result in a lower, stable storage dewar pressure.

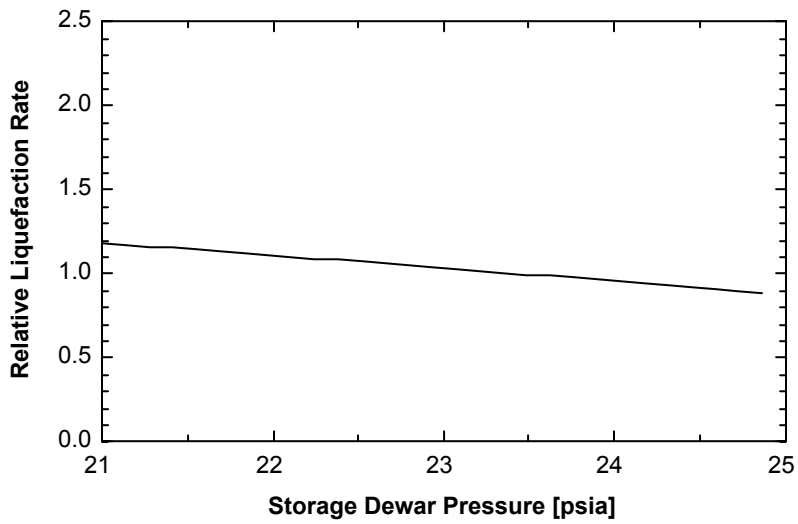

Figure 5 Predicted relative liquefaction rate as a function of storage dewar pressure.

3.3 Turbine Performance

Figures 6 and 7 show the predicted effect of T1 and T2 turbine operations, respectively, on relative liquefaction rate when operating in liquefier mode. Maximizing the isentropic efficiency of both turbines maximizes the liquefaction rate. This is accomplished by running the turbines at high speeds and minimizing system contamination to prevent clogging of the turbine inlet filters.

Given the relative power removal of each turbine (3-4 kW for T1, 0.5-1 kW for T2), it is surprising that the T2 isentropic efficiency appears to have just as large of an effect on liquefaction rate as the T1 isentropic efficiency.

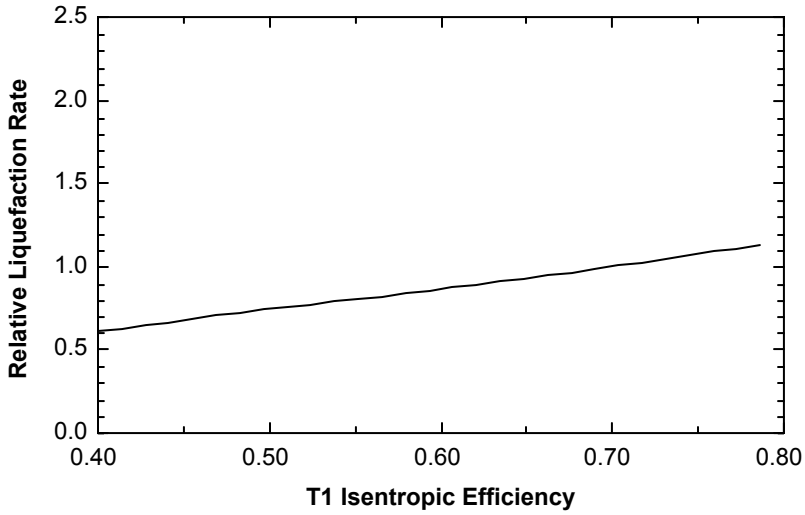

Figure 6 Predicted relative liquefaction rate as a function of T1 turbine isentropic efficiency.

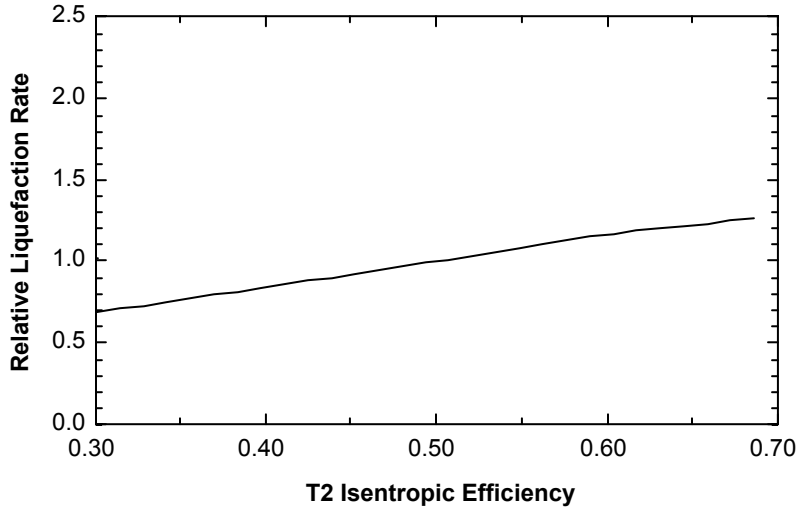

Figure 7 Predicted relative liquefaction rate as a function of T2 turbine isentropic efficiency.

3.4 High-Pressure Stream Temperature at Heat Exchanger HX-1/1A Outlet.

Figure 8 shows the predicted effect of the high-pressure stream temperature at the heat exchanger HX-1/1A outlet on relative liquefaction rate when operating in liquefier mode. This temperature is typically maintained at 108 K by diverting a portion of the high-pressure stream through the external LN_2 precooler. Changing this setpoint by several degrees in either direction has little effect on the liquefaction rate.

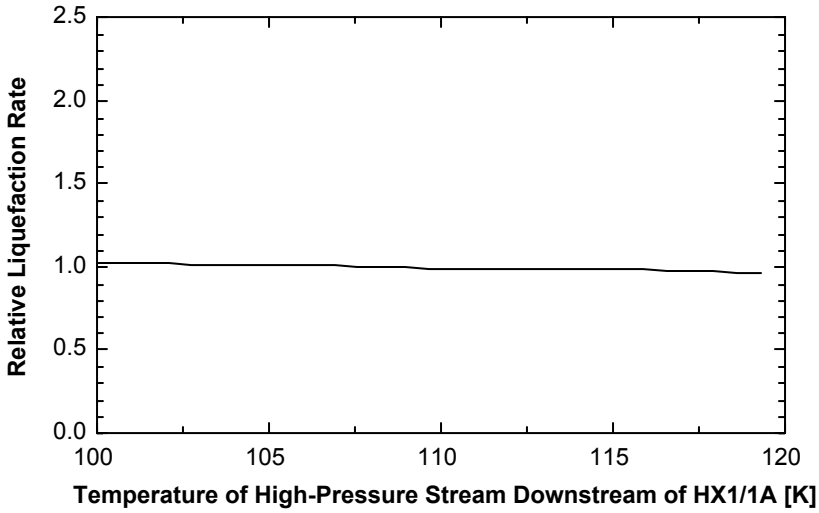

Figure 8 Predicted relative liquefaction rate as a function of the high-pressure stream temperature downstream of heat exchanger HX-1/1A.

3.5 T1 Turbine Outlet Pressure

Figure 9 shows the predicted effect of T1 turbine outlet pressure on relative liquefaction rate when operating in liquefier mode. For each 5 psi drop in the T1 turbine outlet pressure, a 10% increase in the liquefaction rate is predicted.

Reducing the T1 turbine outlet pressure has a number of implications for the compressor system. Decreasing the interstage pressure means that the gas velocity in the first stage oil separator will increase. This issue would need to be carefully studied to verify that the separator would continue to operate properly. Operation of the second stage compressor would be affected, too. Reducing the interstage pressure will actually reduce the second stage motor current by about 15 A at a given discharge pressure. A reduced interstage pressure means there is a larger pressure ratio across the compressor, but this is more than offset by the reduced mass flow. Operation of the gas management system would also need to be studied to verify that the reduced mass flow through the second stage compressor would not result in undue limitations on discharge pressure.

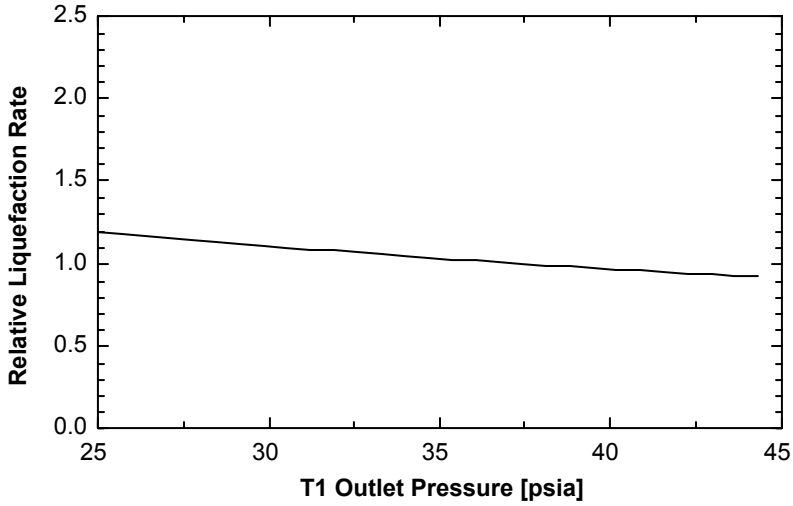

Figure 9 Predicted relative liquefaction rate as a function of T1 turbine outlet pressure.

3.6 T2 Turbine Outlet Pressure

Figure 10 shows the predicted effect of T2 turbine outlet pressure on relative liquefaction rate when operating in liquefier mode. The T2 turbine outlet pressure is typically 47 psia. Changing this pressure by several psi in either direction is predicted to have little impact on the liquefaction rate.

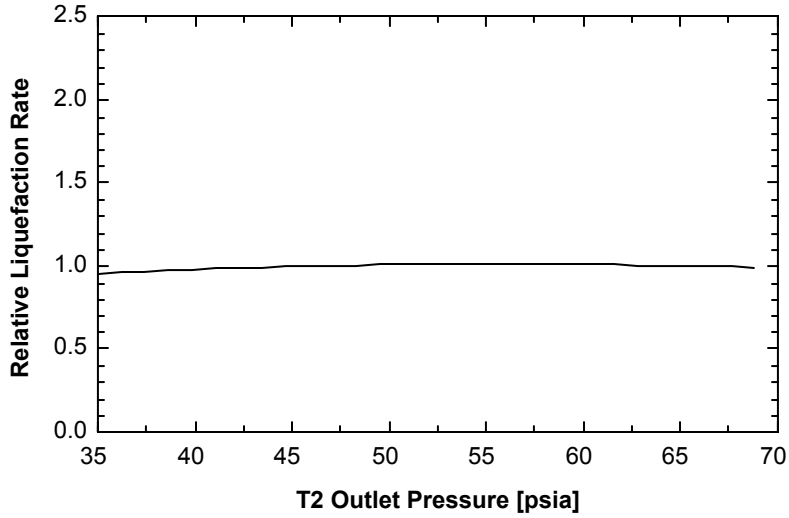

Figure 10 Predicted relative liquefaction rate as a function of T2 turbine outlet pressure.

4. Refrigerator vs. Liquefier Mode

One of the inputs to the cold box model is the cold return flow rate, meaning the model is able to predict system performance when operating in liquefier mode, refrigerator mode,

or in between. The cold return flow is an additional 4.5 K gas flow returning through the low pressure side of the cold box. At MTF, the source of this cold return flow is the distribution box and the Tevatron magnet test stands.

Figure 11 shows the predicted system behavior when operating as a part liquefier, part refrigerator. The horizontal axis is the change in cold return flow rate, and the vertical axis is the change in net liquefaction rate. The model predicts that the net liquefaction rate is reduced by 20% of the change in the cold return flow rate. That is, the net liquefaction rate is reduced by 1 g/s for every additional 5 g/s of liquid helium withdrawn from the storage dewar and returned to the cold box as cold gas. Based on operating experience, the predicted 1:5 ratio is quite accurate. Comparing liquefaction rates on February 12, 2005 with Tevatron test stand 6 online and then offline with identical plant parameters (compressor discharge pressure, storage dewar pressure, turbine operations, T2 bypass valve), a 5.8 g/s change in liquefaction rate resulted from a 26.6 g/s change in cold return flow to the cold box for a ratio of 1:4.6. A line is indicated on Figure 11. Some discrepancy is expected due to operation of the distribution box subcooler, which is not included in these calculations or the model.

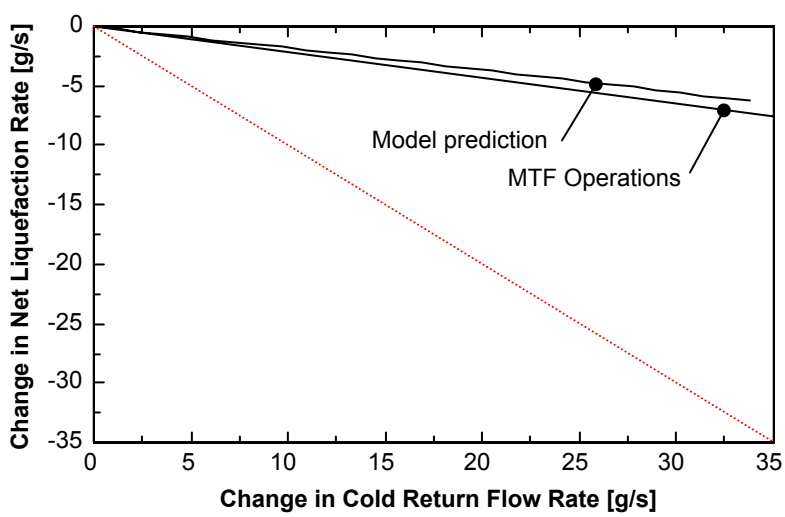

Figure 11 Change in net liquefaction rate vs. change in cold return flow rate predicted by this model and observed in MTF operations.

5. Conclusions

An equation-based model of the cold box has been written. Real component performance parameters (e.g., turbine efficiencies) have been included. The model indicates that compressor discharge pressure and storage dewar pressure are two key parameters for improving system performance. It is believed that the compressor slide valve change-out and automatic operation of control loop PIC300 will allow the liquefaction rate to be maximized while maintaining stable system operations during simultaneous support of

multiple test stands. When possible, the model predictions will be compared against MTF operations data.

Development of the cold box model will continue. The most important limitation of the model is convergence of the equation set. The greatest effect of this convergence problem was the cold box mass flow rate vs. discharge pressure relationship of Figure 2. The mass flow balance among the three process streams within the cold box is not correct because of the low calculated flow rate entering the cold box. It has been determined that in some cases this convergence problem can be traced to the heat exchanger model. Determining which process stream has the minimum thermal capacitance C_{min} is like a binary function. The process stream identified as having the minimum thermal capacitance changes as the solver iterates and will sometimes prevent the equation set from converging. Further study of multi-stream plate and fin heat exchanger modeling will be carried out and hopefully can be integrated with this model.

References

1. S. A. Klein and F. L. Alvarado, EES – Engineering Equation Solver, F-Chart Software, Middleton, WI, 1997.
2. Cryodata, Inc., Littleton, CO.
3. R. Rabehl, "Operational Characteristics of the MTF Liquid Helium Plant," Fermilab Technical Division note TD-05-007.
4. Xing Luo, Kequn Li, and Meiling Li, "Prediction of the thermal performance of multistream plate-fin heat exchangers," *International Journal of Heat Exchangers*, Volume II (2001), pp. 47-60.
5. R. Boehme, J. A. R. Parise, and R. Pitanga Marques, "Simulation of multistream plate-fin heat exchangers of an air separation unit," *Cryogenics*, Volume 43 (2003), pp. 325-334.
6. R. Rabehl, "Parameter Estimation and the Use of Catalog Data with TRNSYS," MS-Mechanical Engineering thesis, University of Wisconsin-Madison Solar Energy Laboratory, 1997.